Structural Engineering and Mechanics, *Vol. 55, No. 4 (2015) 839-856*
DOI: http://dx.doi.org/10.12989/sem.2015.55.4.839

Helical gear multi-contact tooth mesh load analysis with flexible bearings and shafts

Chengwu Li*, Yulin He[a] and Xianxiong Ning[b]

State Key Lab for Mechanical Transmission, Chongqing University, No. 174 Shazhengjie, Shapingba, Chongqing, P.R. China

(Received March 13, 2013, Revised March 20, 2015, Accepted July 28, 2015)

Abstract. A multi-contact tooth meshing model for helical gear pairs considering bearing and shaft deformations is proposed. First, to easily incorporate into the system model, the complicated Harris' bearing force-displacement relationship is simplified applying a linear least square curve fit. Then, effects of shaft and bearing flexibilities on the helical gear meshing behavior are implemented through transformation matrices which contain the helical gear orientation and spatial displacement under loads. Finally, true contact lines between conjugated teeth are approximated applying a modified meshing equation that includes the influence of tooth flank displacement on the tooth contact induced by shaft and bearing displacements. Based on the model, the bearing's force-displacement relation is examined, and the effects of shaft deformation and external load on the multi-contact tooth mesh load distribution are also analyzed. The advantage of this work is, unlike previous works to search true contact lines through time-consuming iterative strategy, to determine true contact lines between conjugated teeth directly with presentation of deformations of bearings and shafts.

Keywords: helical gear; multi-contact; load analysis

1. Introduction

Helical gear is applied widely in power transmissions and possesses the advantage of having more gradual tooth mesh engagement process than spur gear causing it to run quieter and smoother. With the increased use of helical gear towards high power density and high speed applications, its inherent multi-contact tooth mesh behavior is increasingly of interest to gear engineers and researchers. The relevant studies are described next.

Kolivand and Kahraman (2011) reconstructed the tooth surface as the function of roll angle, and the action surface and roll angle were defined by the positions and normal vectors of points on the mating surfaces and gear's axis vectors as well. For a given of roll angle, the locations and orientations of potential instantaneous contact lines between two mating gear surface were determined. Hotait *et al*. (2007) verified a model to predict gear load distribution and

*Corresponding author, Ph.D. Student, E-mail: chengwulee@cqu.edu.cn
[a]Professor, E-mail: heyulin@cqu.edu.cn
[b]Associate Professor, E-mail: ningxianxiong@163.com

http://www.techno-press.org/?journal=sem&subpage=8 ISSN: 1225-4568 (Print), 1598-6217 (Online)

recommended the magnitude of lead crown with present of misalignment by a serious of experiments which studied the combined influence of shaft misalignments and gear lead crown on the load distribution and tooth bending stresses. Zhang and Fang (1999) proposed an approach to analyze helical gear tooth contact and load distribution, which includes the effects of tooth profile modification, manufacturing error and tooth surface elasticity deformation. Their simulation results revealed that the mesh characteristics of the helical gear with small cross angle are similar to those of parallel-axis helical gear. Chen and Tsay (2001) analyzed the contact ellipses of an involute helical pinion and a modified circular-arc helical gear, and illustrated the effect of double crowns on their point contacts and parabolic transmission errors. Litvin *et al*. (1999, 2003, 2005) proposed the computerized approaches to (i) examine the contact behavior of a pair of helical gear, (ii) analyzed the influence of misalignment on the shift of the bearing, and transmission of helical and double-crowned helical gears, (iii) investigated the point contact of double-crowned pinion with a conventional helical involute tooth profile, and (iv) also simulated the use of profile modification of helical gear to avoid edge contact, and reduce noise and vibration. Baud and Velex (2002) investigated the spur and helical gear tooth loading to validate a finite element code for tooth load analysis. The experiment was conducted with high-precision spur and helical, flexible shaft and hydrostatic or hydrodynamic bearings. The corresponding model uses an iterative contact algorithm to search for tooth flank contact conditions at each integration time step. Hedlund and Lehtovaara (2007) established a 3-dimensional finite element model for helical gear to study its contact behavior that accounts for tooth bending, shearing and tooth foundation flexibility. It was found that tooth foundation flexibility have affect contact load sharing significantly, while contact flexibility plays only a minor role. Wink and Serpa (2008) demonstrated the efficiency of direct matrix solver based on Cholesky factorization in studying load distribution problems in terms of computational effort to solve the load distribution problem and the accuracy of the solution comparing to two other solvers: incremental procedure with gradual and iterative load application and pseudo-interference. Kar and Mohanty (2008) introduced an algorithm in determining the time-varying parameters in a helical gear system. In Kar and Mohanty's study, the contact line variation that is a fundamental gearing parameter is shown to induce other variations such as friction force and torque, bearing reaction load, and mesh stiffness and damping variations. Wu and Tsai (2009) proposed an approach for modeling loaded tooth contact of skew conical gear drivers assuming approximate line contact. The contact behavior was analyzed considering tooth contact and bending deformations. Miyoshi *et al*. (2007) proposed an approach to compute tooth contact load distribution of helical gear under any loading condition. In that study, firstly, helical gear pair tooth flank deformation given an input torque was calculated. Secondly the distributions of both static deformation and load were obtained. Thirdly, the proposed equations were combined to find actual tooth contact load distribution. Vinayak and Singh (1998) established a multi-body dynamics modeling for external, fixed center helical or spur gear considering gear body compliances. They showed that the gear response is governed by a set of non-linear differential equations with time-varying coefficients.

In spite of the vast number of related studies published, it is surprising that there are scarcities of published studies on the helical gear multi-contact tooth mesh loads with considering the flexibilities of shaft and bearing. This study attempts to address this gap in the literatures by examining the contact load distributions of Three-dimensional multi-contact helical gear pair including shaft compliance and bearing deformation. In fact, this study represents an extension of the work reported in Wang *et al*. (2012). The shaft deformation includes both torsional and bending response. On the other hand, the bearing deformation only includes the shaft radial

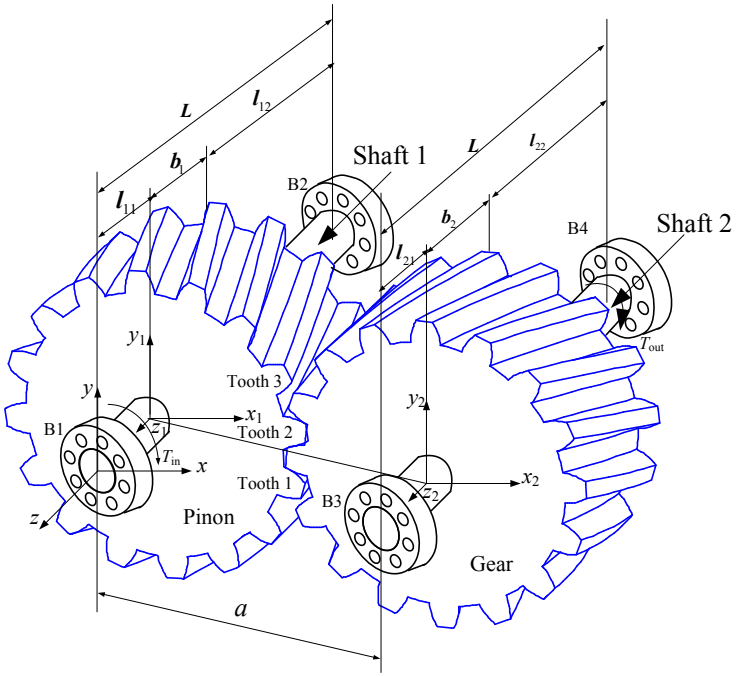

Fig. 1 Schematic diagram of a typical helical gear pair system

displacement. The advantage of the helical gear system modeling proposed in this study is the variation of multi-contact load distribution is coupled with shaft and bearing deformation.

2. Formulations

A typical helical gear system is shown in Fig. 1. Here, both pinion and gear are supported by tapered roller bearings represented by B1, B2, B3 and B4 through shaft 1 and shaft 2 respectively. The global coordinate system xyz has its x-axis directed horizontally to gear, y-axis directed vertically upward and z-axis directed horizontally along the axis of shaft 1. The position of pinion is defined with the local coordinate system $x_1y_1z_1$ and that of gear with the local coordinate system $x_2y_2z_2$. The lengths of shaft 1 and shaft 2 are equal and labeled by L, which is the sum of l_{11}, b_1 and l_{12} for shaft 1 and l_{21}, b_2 and l_{22} for shaft 2. It may be noted that b_1 and b_2 are widths of pinion and gear respectively. The center distance between pinion and gear is denoted by variable a.

The helical gear system of interest to the present analysis is composed of four bearings, two shafts and two gears, which are all assumed to be flexible as shown in Figs. 2(a)-(c). Since the bearing allows free rotation about its axis, its transversal translation degrees of freedom are denoted by $\Delta x_b=\{\Delta x_{bi}\ \Delta x_{bi}\}^T$ (i=1...4) , where the subscript b refers to the bearing, i refers to the number of bearing, and its axial translation degree of freedom is represented by $\Delta z_b=\{\Delta z_{bi}\}^T$ (i=1…4). The shaft is capable of both bending and torsional deformations. The gear translation due to shaft bending deformation is $\Delta \boldsymbol{x}=\{\Delta \boldsymbol{x_i}\ \Delta \boldsymbol{y_i}\}^T$ (i=1, 2), and the rotations of pinion and gear due to shaft torsional deformation are φ_1 and φ_2. Finally, the gear title angle owing to shaft bending deformation are represented with $\boldsymbol{\beta}=\{\beta_{xi}\quad \beta_{yi}\}^T$ (i=1…4).

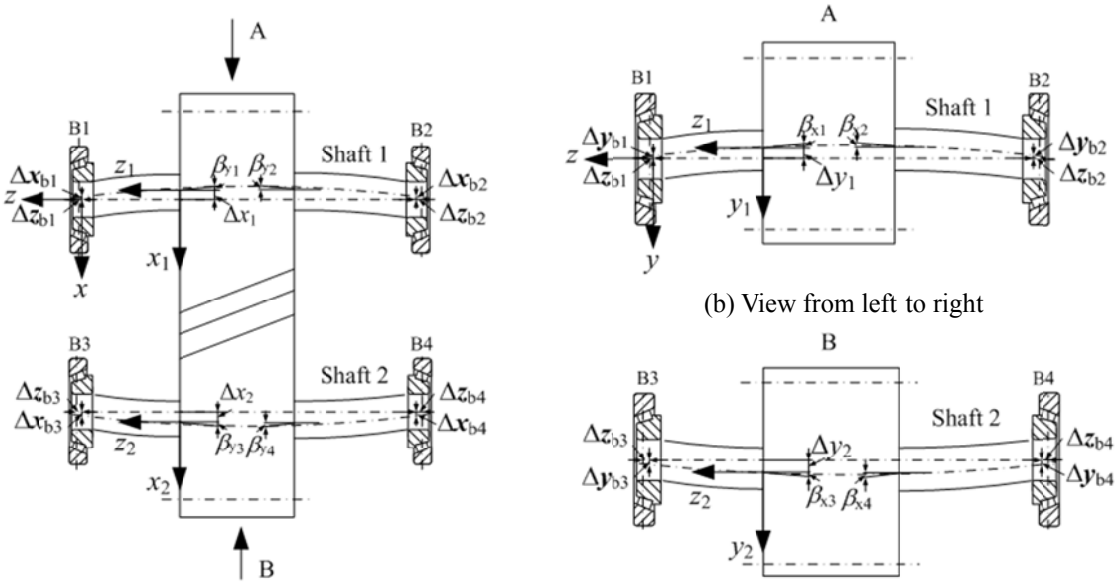

(a) View from top to bottom

(b) View from left to right

(c) View from right to left

Fig. 2 The deformations of the helical gear system

2.1 Bearing model

The relationship between the bearing external load and deformation is given by Harris (2001). For the case when the bearing undertakes combined radial and thrust load

$$F_{\mathrm{r}} = z_{\mathrm{b}} Q_{\max} J_{\mathrm{r}}(\varepsilon)\cos\alpha \tag{1a}$$

$$F_{\mathrm{a}} = z_{\mathrm{b}} Q_{\max} J_{\mathrm{a}}(\varepsilon)\sin\alpha \tag{1b}$$

$$\boldsymbol{J}_{\mathrm{r}}(\boldsymbol{\varepsilon}) = \frac{1}{2\pi}\int_{-\psi_1}^{\psi_1}[1-\frac{1}{2\boldsymbol{\varepsilon}}(1-\cos\boldsymbol{\psi})]^{n}\cos\boldsymbol{\psi}\mathrm{d}\psi \qquad (n=10/9 \text{ for roller bearing}) \tag{1c}$$

$$J_{\mathrm{a}}(\varepsilon) = \frac{1}{2\pi}\int_{-\psi_1}^{\psi_1}[1-\frac{1}{2\varepsilon}(1-\cos\psi)]^{n}\mathrm{d}\psi \qquad (n=10/9 \text{ for roller bearing}) \tag{1d}$$

$$\boldsymbol{\psi}_1 = \cos^{-1}(-\frac{\Delta z_{\mathrm{b}}\tan\boldsymbol{\alpha}}{\Delta \boldsymbol{r}_{\mathrm{b}}}) \tag{1e}$$

$$\boldsymbol{\varepsilon} = \frac{1}{2}(1+\frac{\Delta z_{\mathrm{b}}\tan\boldsymbol{\alpha}}{\Delta \boldsymbol{r}_{\mathrm{b}}}) \tag{1f}$$

$$Q_{\max} = 4.08F_{\mathrm{r}}/z_{\mathrm{b}}\cos\alpha \tag{1g}$$

where F_r and F_a are bearing radial and thrust loads, z_b is the number of rollers, $Q_{\max}$ is the

maximum roller normal load, α is roller contact angle, and Δr_b and Δz_b are bearing radial and axial displacements respectively.

From the above set of equations, the bearing radial load F_r and thrust load F_a appear to be complex functions of the bearing radial displacement $\Delta \boldsymbol{r}_b$ and axial displacement $\Delta \boldsymbol{z}_b$. In fact, as it is demonstrated below, the bearing loads have a nearly linear relationship with their deformation, and thus, a simple relationship between bearing load and deformation can be developed employing the least square method. Firstly, the bearing radial displacement $\Delta \boldsymbol{r}_b$ and axial displacement $\Delta \boldsymbol{z}_b$ are discretized based on the intervals noted by

$$\Delta \overline{\boldsymbol{r}}_{\mathrm{b}} = \left\{ \Delta \overline{r}_{\mathrm{b}1} \quad \Delta \overline{r}_{\mathrm{b}2} \quad \ldots \quad \Delta \overline{r}_{\mathrm{b}m} \right\}^{\mathrm{T}} \tag{2a}$$

$$\Delta \overline{\boldsymbol{z}}_{\mathrm{b}} = \left\{ \Delta \overline{z}_{\mathrm{b}1} \quad \Delta \overline{z}_{\mathrm{b}2} \quad \ldots \quad \Delta \overline{z}_{\mathrm{b}m} \right\}^{\mathrm{T}} \tag{2b}$$

Substitution of the above values into Eqs. 1(a-g) to yield the corresponding bearing radial load $\overline{\boldsymbol{F}}_r$ and thrust load $\overline{\boldsymbol{F}}_a$ whose rows correspond to the variation of the radial displacement $\Delta \overline{\boldsymbol{r}}_{\mathrm{b}}$ and the columns related to the variation of axial displacement $\Delta \overline{\boldsymbol{z}}_{\mathrm{b}}$,

$$\overline{\mathbf{F}}_{\mathrm{r}} = \begin{bmatrix} \overline{F}_{\mathrm{r}11} & \overline{F}_{\mathrm{r}12} & \ldots & \overline{F}_{\mathrm{r}1m} \\ \overline{F}_{\mathrm{r}21} & \overline{F}_{\mathrm{r}22} & \ldots & \overline{F}_{\mathrm{r}2m} \\ \ldots & \ldots & \ldots & \ldots \\ \overline{F}_{\mathrm{r}m1} & \overline{F}_{\mathrm{r}m2} & \ldots & \overline{F}_{\mathrm{r}mm} \end{bmatrix} \tag{3a}$$

$$\overline{\mathbf{F}}_{\mathrm{a}} = \begin{bmatrix} \overline{F}_{\mathrm{a}11} & \overline{F}_{\mathrm{a}12} & \ldots & \overline{F}_{\mathrm{a}1m} \\ \overline{F}_{\mathrm{a}21} & \overline{F}_{\mathrm{a}22} & \ldots & \overline{F}_{\mathrm{a}2m} \\ \ldots & \ldots & \ldots & \ldots \\ \overline{F}_{\mathrm{a}m1} & \overline{F}_{\mathrm{a}m2} & \ldots & \overline{F}_{\mathrm{a}mm} \end{bmatrix} \tag{3b}$$

Simultaneously, bearing radial load F_r and thrust load F_a are expressed as linear functions of the bearing radial displacement Δr_b and axial displacement Δz_b given by

$$F_{\mathrm{r}} = k_{\mathrm{rr}} \Delta r_{\mathrm{b}} + k_{\mathrm{ra}} \Delta z_{\mathrm{b}} + F_{\mathrm{r}0} \tag{4a}$$

$$F_{\mathrm{a}} = k_{\mathrm{ar}} \Delta r_{\mathrm{b}} + k_{\mathrm{aa}} \Delta z_{\mathrm{b}} + F_{\mathrm{a}0} \tag{4b}$$

Since above equations are simple and closely equivalent to Eqs. 1(a-g), they can be easily incorporated into the system governing equation. Hence, stiffness k_{rr}, k_{ra} and F_{r0} are given as

$$\begin{Bmatrix} k_{\mathrm{rr}} \\ k_{\mathrm{ra}} \\ F_{\mathrm{r}0} \end{Bmatrix} = \left(\sum_{i=1}^{m} \sum_{j=1}^{m} \begin{bmatrix} \Delta \overline{r}_{\mathrm{b}i}^{2} & \Delta \overline{r}_{\mathrm{b}i} \Delta \overline{z}_{\mathrm{b}j} & \Delta \overline{r}_{\mathrm{b}i} \\ \Delta \overline{r}_{\mathrm{b}i} \Delta \overline{z}_{\mathrm{b}j} & \Delta \overline{z}_{\mathrm{b}j}^{2} & \Delta \overline{z}_{\mathrm{b}j} \\ \Delta \overline{r}_{\mathrm{b}i} & \Delta \overline{z}_{\mathrm{b}j} & 1 \end{bmatrix} \right)^{-1} \left(\sum_{i=1}^{m} \sum_{j=1}^{m} \overline{F}_{\mathrm{r}ij} \begin{Bmatrix} \Delta \overline{r}_{\mathrm{b}i} \\ \Delta \overline{z}_{\mathrm{b}j} \\ 1 \end{Bmatrix} \right) \tag{5a}$$

Similarly, the stiffness k_{ar}, k_{aa} and F_{a0} are

$$\begin{Bmatrix} k_{\mathrm{ar}} \\ k_{\mathrm{aa}} \\ F_{\mathrm{a0}} \end{Bmatrix} = \left(\sum_{i=1}^{m} \sum_{j=1}^{m} \begin{bmatrix} \Delta\overline{r}_{\mathrm{b}i}^{2} & \Delta\overline{r}_{\mathrm{b}i}\Delta\overline{z}_{\mathrm{b}j} & \Delta\overline{r}_{\mathrm{b}i} \\ \Delta\overline{r}_{\mathrm{b}i}\Delta\overline{z}_{\mathrm{b}j} & \Delta\overline{z}_{\mathrm{b}j}^{2} & \Delta\overline{z}_{\mathrm{b}j} \\ \Delta\overline{r}_{\mathrm{b}i} & \Delta\overline{z}_{\mathrm{b}j} & 1 \end{bmatrix} \right)^{-1} \left(\sum_{i=1}^{m} \sum_{j=1}^{m} \overline{F}_{\mathrm{a}ij} \begin{Bmatrix} \Delta\overline{r}_{\mathrm{b}i} \\ \Delta\overline{z}_{\mathrm{b}j} \\ 1 \end{Bmatrix} \right) \tag{5b}$$

If the bearing reaction loads are decomposed into F_x, F_y and F_z components along the x-axis, y-axis and z-axis respectively, the bearing radial reaction load can be written as

$$F_{\mathrm{r}} = \sqrt{F_{\mathrm{x}}^{2} + F_{\mathrm{y}}^{2}} \tag{6}$$

Then, the bearing radial displacement Δr_b and axial displacement Δz_b are

$$\begin{Bmatrix} \Delta r_{\mathrm{b}} \\ \Delta z_{\mathrm{b}} \end{Bmatrix} = \begin{bmatrix} k_{\mathrm{rr}} & k_{\mathrm{ra}} \\ k_{\mathrm{ar}} & k_{\mathrm{aa}} \end{bmatrix}^{-1} \left(\begin{Bmatrix} F_{\mathrm{r}} \\ F_{\mathrm{a}} \end{Bmatrix} - \begin{Bmatrix} F_{\mathrm{r0}} \\ F_{\mathrm{a0}} \end{Bmatrix} \right) \tag{7}$$

Finally, bearing transversal translation degrees of freedom are expressed as

$$\Delta \boldsymbol{x}_{\mathrm{b}} = \begin{Bmatrix} \Delta x_{\mathrm{b}} \\ \Delta y_{\mathrm{b}} \end{Bmatrix} = \frac{\Delta r_{\mathrm{b}}}{F_{\mathrm{r}}} \begin{Bmatrix} F_{\mathrm{x}} \\ F_{\mathrm{y}} \end{Bmatrix} \tag{8}$$

2.2 Shaft model

The purpose of shaft is to transmit torque between the components in the system. The loads acting on the shaft is shown in Fig. 3. The illustration shows the loads acting on shaft 1, which are the distributed contact load $\boldsymbol{P}=\{p_1\ p_2\ \ldots\ p_m\ p_{m+1}\ \ldots\ p_n\}^{\mathrm{T}}$, the reaction load $\boldsymbol{F}_{b1}=\{F_{bx1}\ F_{by1}\ F_{bz1}\}^{T}$on the shaft 1 at bearing B1 in the transverse plane, and the reaction load $\boldsymbol{F}_{b2}=\{F_{bx2}\ F_{by2}\ F_{bz2}\}^{T}$ at bearing B2. Since it is a statically determined system, the bearing reaction load $\boldsymbol{F}_{b2}$ and $\boldsymbol{F}_{b2}$ may be obtained from the equations of static equilibrium

$$\boldsymbol{F}_{\mathrm{b1}} + \boldsymbol{F}_{\mathrm{b2}} - \mathbf{n} \cdot \boldsymbol{P} = 0 \tag{9a}$$

$$\boldsymbol{F}_{\mathrm{b1}} \times \boldsymbol{L} - \left(\mathbf{n} \cdot \boldsymbol{P}\right) \times (\boldsymbol{L} - \boldsymbol{z}) = 0 \tag{9b}$$

where $\boldsymbol{n}$ is a matrix that comprises of unit column vectors normal to the tooth surfaces at the contact points. Also, $\boldsymbol{L}=\{0\ 0\ L\}^{T}$ and $\boldsymbol{z}$ is a vector storing the z-coordinate of the contact points. Solving Eqs. 9(a-b) simultaneously yields

$$\boldsymbol{F}_{\mathrm{b1}} = \left(\mathbf{n} \cdot \boldsymbol{P}\right) \times (\boldsymbol{L} - \boldsymbol{z}) / L \tag{10a}$$

$$\boldsymbol{F}_{\mathrm{b2}} = \mathbf{n} \cdot \boldsymbol{P} - \left(\mathbf{n} \cdot \boldsymbol{P}\right) \times (\boldsymbol{L} - \boldsymbol{z}) / L \tag{10b}$$

After the bearing reaction loads $\boldsymbol{F}_{b2}$ and $\boldsymbol{F}_{b2}$ are determined as described above, the shaft deformations are examined next. The shafts may have both bending and torsional deformations. The bending deformation of shaft 1 can be expressed as

$$\begin{cases} \dfrac{d^2\Delta \boldsymbol{x}}{dz^2} = -\dfrac{\boldsymbol{F}_{\mathrm{b1}}}{E_{\mathrm{s}}I_{\mathrm{s}}}z & 0 \le z \le l_1 \\ \dfrac{d^2\Delta \boldsymbol{x}}{dz^2} = -\dfrac{\boldsymbol{F}_{\mathrm{b2}}}{E_{\mathrm{s}}I_{\mathrm{s}}}(L-z) & l_1 + b \le z \le L \end{cases} \tag{11}$$

where E_s is the modulus of elasticity of the shaft and I_s the area moment of inertia. Integrating the above equations with respect to the z-coordinate and assuming the rotation angles at bearings are zero, and then the rotation angle of shaft 1 is

$$\begin{cases} \dfrac{d\Delta \boldsymbol{x}}{dz} = \boldsymbol{\beta}_1 = -\dfrac{\boldsymbol{F}_{\mathrm{b1}}}{2E_{\mathrm{s}}I_{\mathrm{s}}}z^2 & 0 \le z \le l_1 \\ \dfrac{d\Delta \boldsymbol{x}}{dz} = \boldsymbol{\beta}_2 = \dfrac{\boldsymbol{F}_{\mathrm{b2}}}{2E_{\mathrm{s}}I_{\mathrm{s}}}(z^2 - 2Lz + L^2) & l_1 + b \le z \le L \end{cases} \tag{12}$$

Integrating Eq. (12) further yields the displacement of shaft 1 due to its bending deformation

$$\begin{cases} \Delta \boldsymbol{x} = -\dfrac{\boldsymbol{F}_{\mathrm{b1}}}{6E_{\mathrm{s}}I_{\mathrm{s}}}z^3 + \Delta \boldsymbol{x}_{\mathrm{b1}} & 0 \le z \le l_1 \\ \Delta \boldsymbol{x} = \dfrac{\boldsymbol{F}_{\mathrm{b2}}}{6E_{\mathrm{s}}I_{\mathrm{s}}}(z^3 - 3Lz^2 + 3L^2z - L^3) + \Delta \boldsymbol{x}_{\mathrm{b2}} & l_1 + b \le z \le L \end{cases} \tag{13}$$

Similar expressions can also be obtained for shaft 2 just by changing the sign of contact load $\boldsymbol{P}$.

Finally, the oriental varying of pinion and gear brought by the shaft bending deformation are given as

$$\begin{Bmatrix} \beta_{\mathrm{y1}} \\ \beta_{\mathrm{x1}} \end{Bmatrix}_{z=l_1} = -\frac{\boldsymbol{F}_{\mathrm{b1}}}{2E_{\mathrm{s}}I_{\mathrm{s}}}l_1^2 \qquad \begin{Bmatrix} \beta_{\mathrm{y2}} \\ \beta_{\mathrm{x2}} \end{Bmatrix}_{z=L-l_2} = \frac{\boldsymbol{F}_{\mathrm{b2}}}{2E_{\mathrm{s}}I_{\mathrm{s}}}l_2^2 \tag{14a-b}$$

$$\begin{Bmatrix} \beta_{\mathrm{y3}} \\ \beta_{\mathrm{x3}} \end{Bmatrix}_{z=l_1} = -\frac{\boldsymbol{F}_{\mathrm{b3}}}{2E_{\mathrm{s}}I_{\mathrm{s}}}l_1^2 \qquad \begin{Bmatrix} \beta_{\mathrm{y4}} \\ \beta_{\mathrm{x4}} \end{Bmatrix}_{z=L-l_2} = \frac{\boldsymbol{F}_{\mathrm{b4}}}{2E_{\mathrm{s}}I_{\mathrm{s}}}l_2^2 \tag{14c-d}$$

The displacements of the pinion and gear caused by the shaft bending deformation are

$$\begin{Bmatrix} \Delta x_1 \\ \Delta y_1 \end{Bmatrix}_{z=l_1} = -\frac{\boldsymbol{F}_{\mathrm{b1}}}{6E_{\mathrm{s}}I_{\mathrm{s}}}l_1^3 + \Delta \boldsymbol{x}_{\mathrm{b1}} \qquad \begin{Bmatrix} \Delta x_2 \\ \Delta y_2 \end{Bmatrix}_{z=l_1} = -\frac{\boldsymbol{F}_{\mathrm{b3}}}{6E_{\mathrm{s}}I_{\mathrm{s}}}l_1^3 + \Delta \boldsymbol{x}_{\mathrm{b3}} \tag{15a-b}$$

For shaft torsional deformation, the expressions are given by

$$\varphi_1 = \frac{T_{in}l_1}{GI_1} \qquad \varphi_2 = \frac{T_{out}l_2}{GI_2} \tag{16a-b}$$

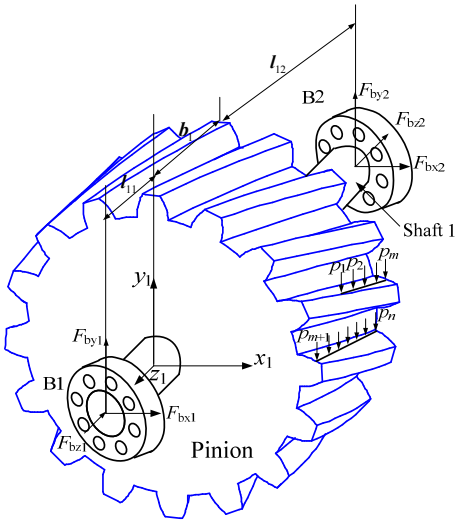

Fig. 3 Contact load acting on the pinion along with the reaction load on the shaft 1

2.3 The transformation matrix

In this study, the most critical task is to couple the deformation of the bearings and shafts and the contact behavior of pinion and gear. This is accomplished with two transformation matrices $\mathbf{T}_1$ and $\mathbf{T}_2$. The transformation matrix $\mathbf{T}_1$ transfers pinion contact behavior defined by the coordinate $x_1y_1z_1$ to the global coordinate xyz, which contains deformations of both bearing and shaft 1

$$\mathbf{T}_1(\phi_1,\varphi_1,\Delta\beta_{x1},\Delta\beta_{y1},\Delta x_1,\Delta y_1)=\begin{bmatrix} \cos(\phi_1+\varphi_1)\cos\Delta\beta_{y1} & -\sin(\phi_1+\varphi_1)\cos\Delta\beta_{y1} & \sin\Delta\beta_{y1} & \Delta x_1 \\ \sin(\phi_1+\varphi_1)\cos\Delta\beta_{x1}+\cos(\phi_1+\varphi_1)\sin\Delta\beta_{y1}\sin\Delta\beta_{x1} & \cos(\phi_1+\varphi_1)\cos\Delta\beta_{x1}+\sin(\phi_1+\varphi_1)\sin\Delta\beta_{y1}\sin\Delta\beta_{x1} & -\cos\Delta\beta_{y1}\sin\Delta\beta_{x1} & \Delta y_1 \\ \sin(\phi_1+\varphi_1)\sin\Delta\beta_{x1}-\cos(\phi_1+\varphi_1)\sin\Delta\beta_{y1}\cos\Delta\beta_{x1} & \cos(\phi_1+\varphi_1)\sin\Delta\beta_{x1}+\sin(\phi_1+\varphi_1)\sin\Delta\beta_{y1}\cos\Delta\beta_{x1} & \cos\Delta\beta_{y1}\cos\Delta\beta_{x1} & l_1 \\ 0 & 0 & 0 & 1 \end{bmatrix} \tag{17}$$

where ϕ_1 is rigid rotation angle of pinion, $\Delta\beta_{x1}=\beta_{x1}-\beta_{x2}$ and $\Delta\beta_{y1}=\beta_{y1}-\beta_{y2}$.

Similarly, the transformation matrix $\mathbf{T}_2$ transfers the behavior of gear defined by the coordinate $x_2y_2z_2$ to the global coordinate xyz, which includes the bearing and shaft 2 deformations given by

$$\mathbf{T}_2(\phi_2,\varphi_2,\Delta\beta_{x2},\Delta\beta_{y2},\Delta x_2,\Delta y_2)=\begin{bmatrix} \cos(\phi_2+\varphi_2)\cos\Delta\beta_{y2} & -\sin(\phi_2+\varphi_2)\cos\Delta\beta_{y2} & \sin\Delta\beta_{y2} & \Delta x_2 \\ \sin(\phi_2+\varphi_2)\cos\Delta\beta_{x2}+\cos(\phi_2+\varphi_2)\sin\Delta\beta_{y2}\sin\Delta\beta_{x2} & \cos(\phi_2+\varphi_2)\cos\Delta\beta_{x2}+\sin(\phi_2+\varphi_2)\sin\Delta\beta_{y2}\sin\Delta\beta_{x2} & -\cos\Delta\beta_{y2}\sin\Delta\beta_{x2} & \Delta y_2 \\ \sin(\phi_2+\varphi_2)\sin\Delta\beta_{x2}-\cos(\phi_2+\varphi_2)\sin\Delta\beta_{y2}\cos\Delta\beta_{x2} & \cos(\phi_2+\varphi_2)\sin\Delta\beta_{x2}+\sin(\phi_2+\varphi_2)\sin\Delta\beta_{y2}\cos\Delta\beta_{x2} & \cos\Delta\beta_{y2}\cos\Delta\beta_{x2} & l_2 \\ 0 & 0 & 0 & 1 \end{bmatrix}$$

$$\begin{bmatrix} -\sin(\phi_2+\varphi_2)\cos\Delta\beta_{y2} & \sin\Delta\beta_{y2} & \Delta x_2+a \\ \cos(\phi_2+\varphi_2)\cos\Delta\beta_{x2}+\sin(\phi_2+\varphi_2)\sin\Delta\beta_{y2}\sin\Delta\beta_{x2} & -\cos\Delta\beta_{y2}\sin\Delta\beta_{x2} & \Delta y_2 \\ \cos(\phi_2+\varphi_2)\sin\Delta\beta_{x2}+\sin(\phi_2+\varphi_2)\sin\Delta\beta_{y2}\cos\Delta\beta_{x2} & \cos\Delta\beta_{y2}\cos\Delta\beta_{x2} & l_1 \\ 0 & 0 & 1 \end{bmatrix} \tag{18}$$

where ϕ_2 is rigid rotation angle of gear, $\Delta\beta_{x2}=\beta_{x3}-\beta_{x4}$ and $\Delta\beta_{y2}=\beta_{y3}-\beta_{y4}$.

2.4 Gear model

The details of the gear model are given in Litvin and Fuentes (2004), and therefore only a brief description is described below as a review. For a pair of helical gear with right hand shown in Fig. 1, the tooth profile Σ_1 on the pinion within the coordinate system $x_1y_1z_1$ is expressed as parameters θ_1 and u_1

$$\boldsymbol{r}_1^{'}=\begin{Bmatrix} x_1^{'} \\ y_1^{'} \\ z_1^{'} \end{Bmatrix}=\begin{Bmatrix} r_{b1}\cos(\theta_1+\mu_1)+u_1\cos\lambda_{b1}\sin(\theta_1+\mu_1) \\ -r_{b1}\sin(\theta_1+\mu_1)+u_1\cos\lambda_{b1}\cos(\theta_1+\mu_1) \\ u_1\sin\lambda_{b1}-p_1\theta_1 \end{Bmatrix} \tag{19a}$$

and the unit differential with respect to θ_1 and u_1 are, respectively

$$\boldsymbol{r}_{1\theta}^{'}=\frac{\partial\boldsymbol{r}_1^{'}}{\partial\theta_1}\Big/\left|\frac{\partial\boldsymbol{r}_1^{'}}{\partial\theta_1}\right|=\begin{Bmatrix} \cos(\theta_1+\mu_1) \\ -\sin(\theta_1+\mu_1) \\ 0 \end{Bmatrix} \tag{19b}$$

$$\boldsymbol{r}_{1u}^{'}=\frac{\partial\boldsymbol{r}_1^{'}}{\partial u_1}\Big/\left|\frac{\partial\boldsymbol{r}_1^{'}}{\partial u_1}\right|=\begin{Bmatrix} \cos\lambda_{b1}\sin(\theta_1+\mu_1) \\ \cos\lambda_{b1}\cos(\theta_1+\mu_1) \\ \sin\lambda_{b1} \end{Bmatrix} \tag{19c}$$

The unit normal to the tooth surface Σ_1 is given by

$$\boldsymbol{n}_1^{'}=-\frac{\boldsymbol{r}_{1u}^{'}\times\boldsymbol{r}_{1\theta}^{'}}{\left|\boldsymbol{r}_{1u}^{'}\times\boldsymbol{r}_{1\theta}^{'}\right|}=\begin{Bmatrix} -\sin\lambda_{b1}\sin(\theta_1+\mu_1) \\ -\sin\lambda_{b1}\cos(\theta_1+\mu_1) \\ \cos\lambda_{b1} \end{Bmatrix} \tag{19d}$$

where p_1 is the screw parameter, $\mu_1=w_{t1}/2r_{p1}-\text{inv}\alpha_{t1}$, w_{t1} is the nominal value of space width on the pitch circle, and α_{t1} is the profile angle in the cross section at the point of intersection of the profile with pitch circle. Also, λ_{b1} is the lead angle.

The profile Σ_2 on the gear within the coordinate system $x_2y_2z_2$is expressed as parameters θ_2 and u_2, and its differentials and unit normal are, respectively

$$\boldsymbol{r}_2^{'}=\begin{Bmatrix}x_2^{'}\\y_2^{'}\\z_2^{'}\end{Bmatrix}=\begin{Bmatrix}r_{\mathrm{b}2}\cos(\theta_2-\varepsilon_2)+u_2\cos\lambda_{\mathrm{b}2}\sin(\theta_2-\varepsilon_2)\\-r_{\mathrm{b}2}\sin(\theta_2-\varepsilon_2)-u_2\cos\lambda_{\mathrm{b}2}\cos(\theta_2-\varepsilon_2)\\-u_2\sin\lambda_{\mathrm{b}2}+p_2\theta_2\end{Bmatrix} \tag{20a}$$

$$\boldsymbol{r}_{2\theta}^{'}=\frac{\partial\boldsymbol{r}_2^{'}}{\partial\theta_2}\Big/\left|\frac{\partial\boldsymbol{r}_2^{'}}{\partial\theta_2}\right|=\begin{Bmatrix}-\cos(\theta_2-\varepsilon_2)\\\sin(\theta_2-\varepsilon_2)\\0\end{Bmatrix} \tag{20b}$$

$$\boldsymbol{r}_{2\mathrm{u}}^{'}=\frac{\partial\boldsymbol{r}_2^{'}}{\partial u_2}\Big/\left|\frac{\partial\boldsymbol{r}_2^{'}}{\partial u_2}\right|=\begin{Bmatrix}\cos\lambda_{\mathrm{b}2}\sin(\theta_2-\varepsilon_2)\\-\cos\lambda_{\mathrm{b}2}\cos(\theta_2-\varepsilon_2)\\-\sin\lambda_{\mathrm{b}2}\end{Bmatrix} \tag{20c}$$

$$\boldsymbol{n}_2^{'}=-\frac{\boldsymbol{r}_{2\mathrm{u}}^{'}\times\boldsymbol{r}_{2\theta}^{'}}{\left|\boldsymbol{r}_{2\mathrm{u}}^{'}\times\boldsymbol{r}_{2\theta}^{'}\right|}=\begin{Bmatrix}\sin\lambda_{\mathrm{b}2}\sin(\theta_2-\varepsilon_2)\\-\sin\lambda_{\mathrm{b}2}\cos(\theta_2-\varepsilon_2)\\\cos\lambda_{\mathrm{b}2}\end{Bmatrix} \tag{20d}$$

The contact behavior of helical gear pair is examined within the global coordinate *xyz*, therefore the expressions for tooth profile Σ_1 and Σ_2 of pinion and gear are required to be defined within the global coordinate *xyz* while they must include the influence of bearing and shaft deformation. It is easily accomplished by multiplying the transformation matrix with the expressions for tooth profile Σ_1 and Σ_2 at local coordinate

$$\boldsymbol{r}_1=\mathbf{T}_1(\phi_1,\varphi_1,\Delta\beta_{\mathrm{x}1},\Delta\beta_{\mathrm{y}1},\Delta x_1,\Delta y_1)\boldsymbol{r}_1^{'} \tag{21a}$$

$$\boldsymbol{r}_{\theta1}=\mathbf{T}_1(\phi_1,\varphi_1,\Delta\beta_{\mathrm{x}1},\Delta\beta_{\mathrm{y}1},\Delta x_1,\Delta y_1)\boldsymbol{r}_{\theta1}^{'} \tag{21b}$$

$$\boldsymbol{r}_{\mathrm{u}1}=\mathbf{T}_1(\phi_1,\varphi_1,\Delta\beta_{\mathrm{x}1},\Delta\beta_{\mathrm{y}1},\Delta x_1,\Delta y_1)\boldsymbol{r}_{\mathrm{u}1}^{'} \tag{21c}$$

$$\boldsymbol{n}_1=\mathbf{T}_1(\phi_1,\varphi_1,\Delta\beta_{\mathrm{x}1},\Delta\beta_{\mathrm{y}1},\Delta x_1,\Delta y_1)\boldsymbol{n}_1^{'} \tag{21d}$$

$$\boldsymbol{r}_2=\mathbf{T}_2(\phi_2,\varphi_2,\Delta\beta_{\mathrm{x}2},\Delta\beta_{\mathrm{y}2},\Delta x_2,\Delta y_2)\boldsymbol{r}_2^{'} \tag{22a}$$

$$\boldsymbol{r}_{\theta2}=\mathbf{T}_2(\phi_2,\varphi_2,\Delta\beta_{\mathrm{x}2},\Delta\beta_{\mathrm{y}2},\Delta x_2,\Delta y_2)\boldsymbol{r}_{\theta2}^{'} \tag{22b}$$

$$\boldsymbol{r}_{\mathrm{u}2}=\mathbf{T}_2(\phi_2,\varphi_2,\Delta\beta_{\mathrm{x}2},\Delta\beta_{\mathrm{y}2},\Delta x_2,\Delta y_2)\boldsymbol{r}_{\mathrm{u}2}^{'} \tag{22c}$$

$$\boldsymbol{n}_2=\mathbf{T}_2(\phi_2,\varphi_2,\Delta\beta_{\mathrm{x}2},\Delta\beta_{\mathrm{y}2},\Delta x_2,\Delta y_2)\boldsymbol{n}_2^{'} \tag{22d}$$

Applying Eqs. 21(a-d) and Eqs. 22(a-d) above, the positions and their differences with respect to profile parameters of the tooth profiles Σ_1 and Σ_2 are determined, which represent the foundations for analyzing the gear contact behavior. The detailed description for the deformation

calculation of pinion and gear is given in Wang *et al*. (2012).

2.5 Equation of meshing

The deformed tooth profile Σ_1 of pinion and the deformed tooth profile Σ_2 of gear can be expressed as.

$$\boldsymbol{r}^1 = \boldsymbol{r}_1 + \boldsymbol{q}_{\text{tf}}(\theta_1, u_1) \tag{23a}$$

where $\boldsymbol{q}_{\text{tf}}(\theta_1, \mu_1)$ is a polynomial expression that accounts for pinion and gear deformations and are formed by Chebyshev polynomial fit given in Wang *et al*. (2012). In this study, the influence of deformations of bearings and shaft on the mating teeth meshing is manifested through $\boldsymbol{q}_{\text{tf}}(\theta_1, \mu_1)$.

The unit differentials with respect to parameter θ_1 and u_1, assuming the influences of deformation on the modulus are omitted, are given by

$$\boldsymbol{r}_\theta^1 = \boldsymbol{r}_{1\theta} + \frac{\partial \boldsymbol{q}_{\text{tf}}(\theta_1, u_1)}{\partial \theta_1} \tag{23b}$$

$$\boldsymbol{r}_{\text{u}}^1 = \boldsymbol{r}_{1u} + \frac{\partial \boldsymbol{q}_{\text{tf}}(\theta_1, u_1)}{\partial u_1} \tag{23c}$$

$$\boldsymbol{n} = -\frac{\boldsymbol{r}_\theta^1 \times \boldsymbol{r}_{\text{u}}^1}{\left|\boldsymbol{r}_\theta^1 \times \boldsymbol{r}_{\text{u}}^1\right|} = \mathbf{T}\left(\begin{Bmatrix} -\sin\lambda_{\text{b1}} \sin(\theta_1 + \mu_1) \\ -\sin\lambda_{\text{b1}} \cos(\theta_1 + \mu_1) \\ \cos\lambda_{\text{b1}} \end{Bmatrix} + \boldsymbol{r}_{1\theta} \times \frac{\partial \boldsymbol{q}_{\text{tf}}(\theta_1, u_1)}{\partial u_1} + \mathbf{r}_{1u} \times \frac{\partial \boldsymbol{q}_{\text{tf}}(\theta_1, u_1)}{\partial \theta_1}\right) \tag{23d}$$

The expression for the relative velocity between the pinion and the gear may be represented as,

$$\boldsymbol{v}^{12} = (\boldsymbol{\omega}_1 - \boldsymbol{\omega}_2) \times \boldsymbol{r}_1 - \boldsymbol{a} \times \boldsymbol{\omega}_2 \tag{24}$$

where $\boldsymbol{\omega}_1$ and $\boldsymbol{\omega}_2$ are vector of rotation angular velocity and $\boldsymbol{a}$ is the vector of gear center distance. Hence, the equation of meshing is established based on the fact that the scale product between relative velocity and unit normal direction must be orthogonal, that is

$$\boldsymbol{n} \bullet \boldsymbol{v}^{12} = 0 \tag{25}$$

Here, the subscript "1" is omitted for simplicity.

Rearranging the above equation to obtain

$$\begin{aligned} &\underline{\cos(\phi - \theta - \mu) - \cos\alpha_{\text{t}}} \\ &+(\boldsymbol{r}_\theta \times \frac{\partial \boldsymbol{q}_{\text{tf}}(\theta, u)}{\partial u} + \boldsymbol{r}_{\text{u}} \times \frac{\partial \boldsymbol{q}_{\text{tf}}(\theta, u)}{\partial \theta}) \bullet (\mathbf{T}_1[\rho \quad 0 \quad 0]^{\text{T}} - \boldsymbol{r})^{\text{T}} / \sin\lambda_{\text{b}} = 0 \end{aligned} \tag{26}$$

where the first term on the left hand side of the above equation is contributed by the gear rigid body motion, while the second item represents the influence of the pinion elastic deformation, bearing deformation and shaft deformation on the gear mesh.

Table 1 Parameters of the components in the helical gear system of interest

Components	Parameters	Descriptions	values
Bearing parameters (30208)	d_{in}	Bore diameter	40 mm
	d_{out}	Outside diameter	80 mm
	b_b	Width	19.75 mm
	α	Contact angle	30°
	z_b	Roller number	15
	l	Roller length	10 mm
Gear Parameters	m	Modulus	6 mm
	z	Teeth number	16
	α	Pressure angle	20°
	β	Helix angle	15°
	b	Tooth facewidth	60 mm
	v	Poisson ratio	0.29
	E	Elasticity modulus	2.09×10^{11} Pa
	G	Elasticity shear modulus	3.88×10^{10} Pa
Shaft Parameters	I	Section moment of inertia	1.26×10^{-7} m^4
	l_1	length	60 mm
	l_2	length	60 mm

Finally, due to the assumption of small deformation, the gear tooth contact load should be inversely proportional to the deformation on the contact line, that is

$$\boldsymbol{p}_1\boldsymbol{d}_1 = \boldsymbol{p}_2\boldsymbol{d}_2 = ... = \boldsymbol{p}_n\boldsymbol{d}_n \tag{27}$$

where d_i is the separation distance at contact load p_i due to gear deformation. In addition, the sum of all contact load p_i should balance out with the force exerted by the external torque T as expressed below

$$\sum_{i=1}^{n} p_i = T_{in} / r_{b1} \tag{28}$$

where r_{b1} is the base circle radius of pinion.

3. Numerical analysis

For the helical gear system shown in Fig. 1, the parameters of the components such as bearing, shaft and gear are given in Table 1. Both the input torque and output torque are assumed to be 100 Nm. First of all, the displacement and reaction load of the bearing is examined and its stiffness varying with the contact angle studied.

3.1 Bearing deformation characteristics

Bearing deformation is often omitted in past studies of helical gear system analysis, especially

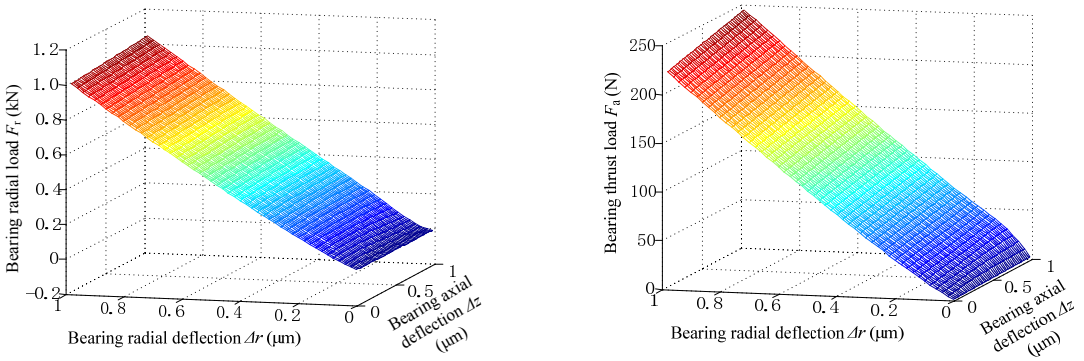

(a) Radial reaction load (b) Thrust reaction load

Fig. 4 Effects of radial and axial deflections on bearing reaction load

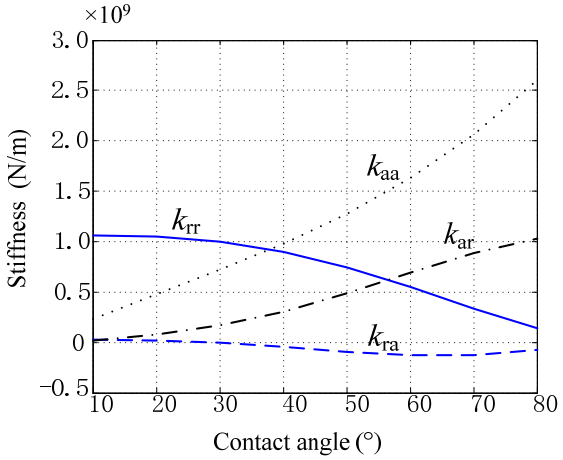

Fig. 5 Effect of contact angle on bearing contact stiffness

in computing the gear contact behavior. Generally speaking, the bearing deformation influences the gear contact behavior in two ways: one is that the bearing deformation causes the gear to rigidly offset from its ideal position; second is that the influence of bearing deformation on the gear rigid offset is generally enlarged due to the shaft leverage function. Therefore, it is useful to investigate bearing deformation characteristics as defined by Eqs. 1(a-g).

Fig. 4 shows the tapered roller bearing radial reaction load F_r (a) and thrust reaction load F_a (b) varying with the radial deflection Δr and axial deflection Δz. During the simulated intervals between 0 and 1 μm of bearing radial deflection and axial deflection, the bearing radial load F_r and thrust reaction load F_a distributed as plane obviously have linear relationship with the radial deflection Δr and axial deflection Δz. As far as the bearing radial load F_r is concerned, it considerably increases from 0 kN to around 1.0 kN with its radial deflection Δr from 0 μm to 1 μm. However, as bearing axial deflection Δz varies within the same interval, the bearing radial reaction load F_r has a slight increase with a scope of 0.1 kN. The bearing thrust reaction load F_r has a similar distribution as the bearing radial reaction load F_a. In summary, the bearing radial reaction load F_r and thrust reaction load F_a grow linearly with the increase of the bearing radial

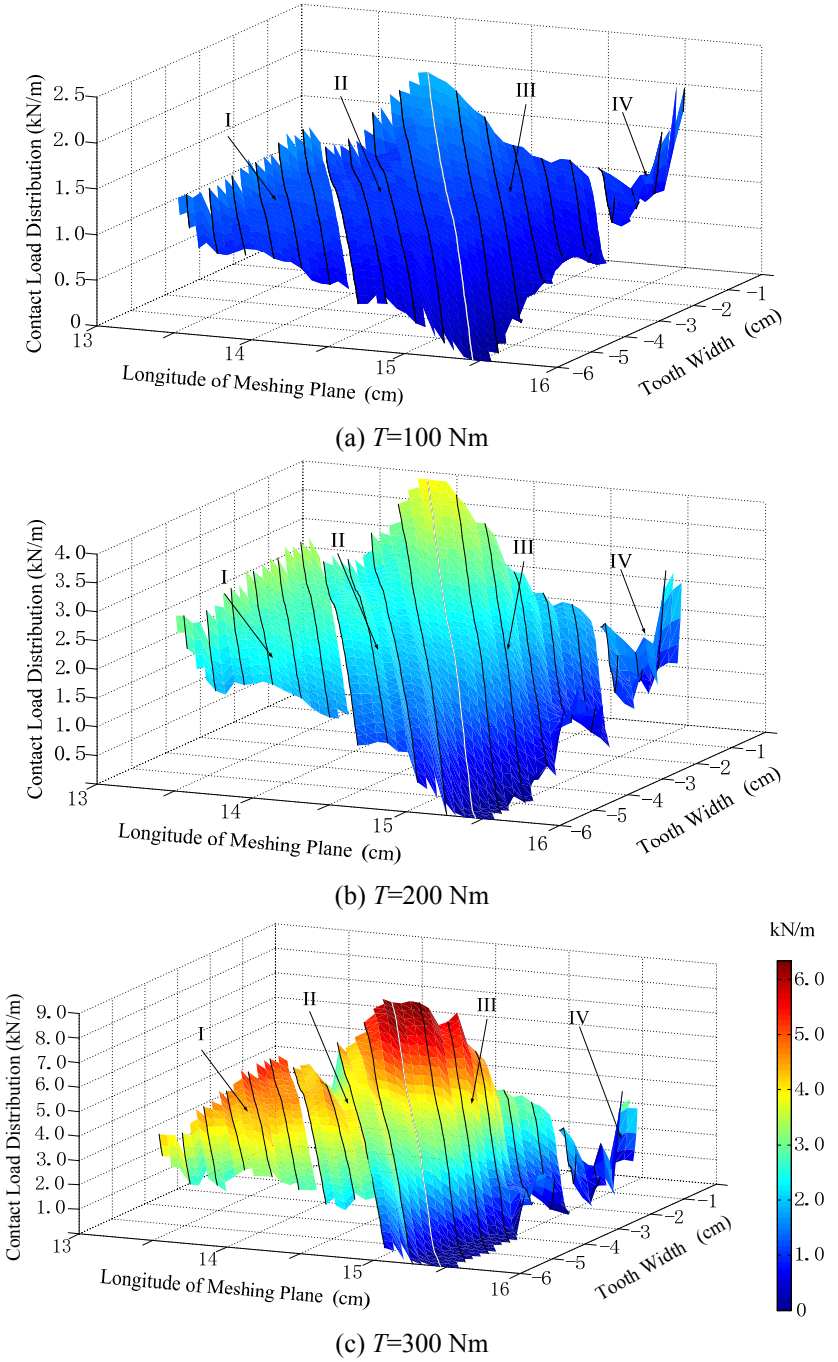

(a) T=100 Nm

(b) T=200 Nm

(c) T=300 Nm

Fig. 6 Contact load distribution in the meshing plane of helical gear pair for roller length of 15 mm, shaft diameter of 20 mm

deflection Δr and axial deflection Δz. As a result, their relationship can be reasonably defined by the linear Eqs. 4(a-b).

The stiffness of tapered roller bearing defined in Eqs. 4(a-b) is illustrated in Fig. 5 as a function of contact angle ranging from 10° to 80°. The stiffness k_{rr} show that the influence of bearing radial deflection Δr on the bearing radial reaction load F_r drops slightly as contact angle rises, while the stiffness k_{ra} has a small value illustrating the weak influence of bearing axial deflection Δz on the bearing radial reaction load F_r. The fact that both the stiffness k_{ra} and k_{aa} increase significantly with the surge of the contact angle shows that, relative to the bearing thrust reaction load F_a, the larger the contact angle, the stiffer the bearing in axes direction.

3.2 Influence of external torque on contact load distribution

As expected, the external torque has a significant impact on the helical gear contact load distribution. Figs. 6(a)-(c) shows the gear contact load distribution in the meshing plane given roller length of 15 mm and shaft diameter of 20 mm for loading condition of 100 Nm, 200 Nm and 300 Nm. There are four sections in the figures indicated by I, II, III and IV to represent the contact load distribution within the meshing plane during a mesh cycle. Tooth pairs 1, 2 and 3, as shown in Fig. 1, are defined as the meshed tooth pairs of Tooth 1, 2 and 3 at the pinion with their corresponding counterparts at the gear. During the designated mesh cycle, the tooth pair 2 is always in contact, while tooth pairs 1 and 3 take part in contact only part of the time. Near the beginning of the meshing cycle shown, the tooth pairs 2 and 1 are in contact simultaneously and their contact load variations are indicated by sections II and IV. Then as the helical gear rotates, the tooth pair 1 disengages while tooth pair 3 engages, and tooth pairs 2 and 3 bear the load simultaneously and their contact load variations are indicated by sections III and I. The thin solid lines represent the contact lines within the meshing plane. The color bar showing the value of contact load for all plots in Fig. 6 is given at the right hand side of Fig. 6(c).

First of all, regardless of the magnitude of external torque, the contact load varies over the tooth flank in a similar approach. At the beginning of the mesh cycle, the tooth pairs 2 and 1 jointly bear the external load. As tooth pair 1 disengages, its contact load fluctuates substantially. Then, as tooth pair 3 comes into contact and carry increasingly more contact load, tooth pair 2 load decreases gradually. Comparing Figs. 6(a)-(c), the maximum contact loads occur at the root of tooth pair 2 as the tooth pair 1 disengages and tooth pair 3 engages, increase from 1.876 kN/m, 3.876 kN/m to 6.338 kN/m corresponding to the external torque 100 Nm, 200 Nm and 300 Nm exerted on the helical gear pair. This behavior obviously demonstrates that the external load has a critical impact on the contact load of helical gear. In addition, unlike past studies that shows the contact load to vary smoothly over the meshing plane, the contact load in this case changes abruptly since not only the effect of bearing radial deformation and shaft torsional deformation are considered as in many past efforts, the shaft bending deformation is also included in this proposed analysis. Finally, the contact load distribution once again shows that the tooth acts like a cantilever beam during meshing due to the fact that the largest contact load appears at the tooth root while the smallest contact load occur at tooth tip.

3.3 Influence of shaft flexibility on contact load distribution

In this section, the influence of shaft flexibility on the contact load distribution is examined. First, the contact load distribution of helical gear for external torque of 100Nm, roller length of 15 mm and shaft diameter of 20 mm is computed and illustrated in Fig. 7(a). The difference of contact load distribution with external torque of 100 N.m and roller length of 15 mm is shown in Fig. 7(b)

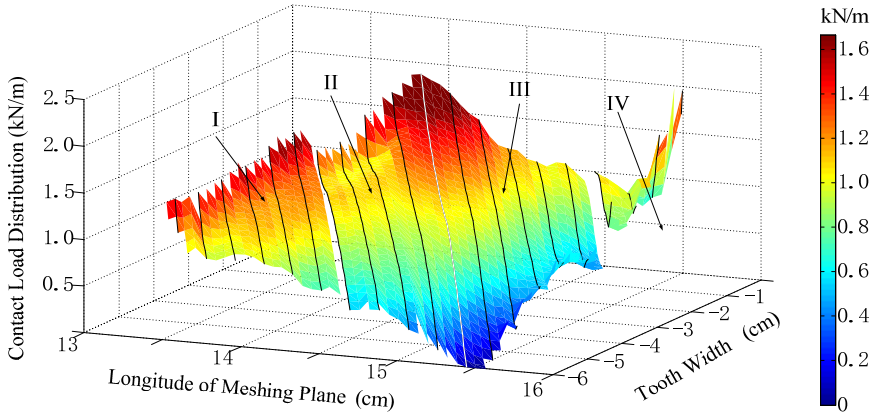

(a) Contact load distribution for T=100 Nm, roller length 15 mm and shaft diameter 20 mm

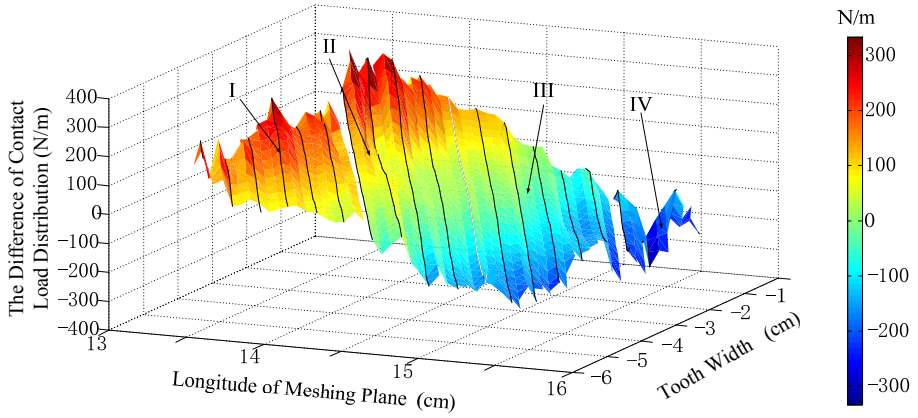

(b) Difference of contact load distribution between shaft diameters of 20 mm and 30 mm

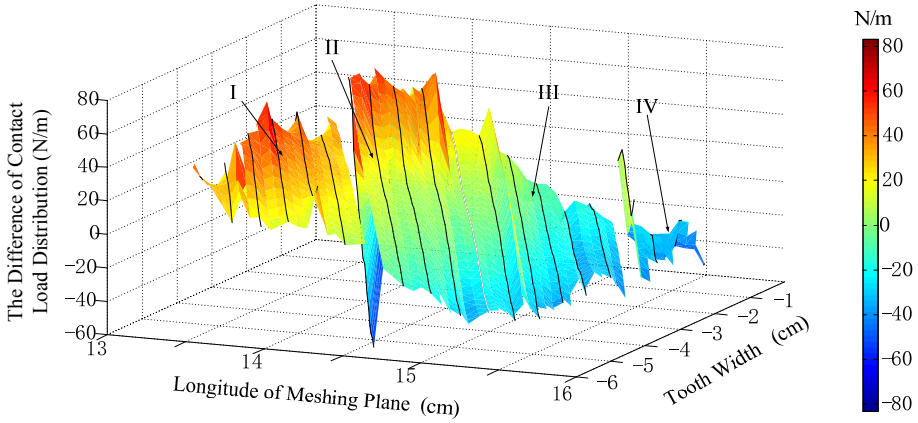

(c) difference of contact load distribution between shaft diameters of 30 mm and 40 mm

Fig. 7 Influence of shaft flexibility on the helical gear contact load distribution in the meshing plane

between shaft diameters of 20 mm and 30 mm; finally, the difference of contact load distribution is given in Fig. 7(c) between shaft diameter 30 mm and 40 mm.

The differences of contact load distributions for different shaft diameters have similar trends over the whole meshing plane. Here, it can be seen that as we get nearer to the tooth root, the larger the difference in contact load is observed. On the other hand, the nearer to the tooth tip, the smaller the difference is observed. In addition, by comparing Fig. 7(b) and Fig. 7(c), it is obvious that the shaft flexibility do not influence linearly on the contact load. For instance, the largest distributed contact load difference between shaft diameter of 20 mm and 30 mm approaches 300 Nm while that between shaft of 30 mm and 40 mm shrinks to only around 80 Nm. This phenomenon demonstrates that the shaft elasticity has a significant impact on the contact load distribution as the shaft becomes more flexible. However, the influence of the shaft elasticity on the contact load distribution decreases significantly as the shaft becomes stiff beyond a certain value. In another word, when the shaft becomes stiffer over a certain value, it is not an effective method to improve the contact load distribution by enlarging the shaft diameter.

4. Conclusions

The contact load distributions of helical gears considering the flexibilities of bearing and shafts are examined using a set of modified mesh equation. The detailed modeling for bearing and shaft are established. Instead of searching the whole tooth flank iteratively, the real contact lines are determined by simply solving the modified mesh equation. The analysis shows that bearing reaction forces is linear with respect to the deformations, the external load has a decided impact on the helical gear contact load and finally shaft exerts a significant influence on the contact load when shaft is flexible, however, as the shaft become stiff, this influence decreases considerably.

References

Baud, S. and Velex, P. (2002), "Static and dynamic tooth loading in spur and helical geared systems-experiments and model validation", *J. Mech. Des*., **124**, 334-346.

Chen, Y.C. and Tsay, C.B. (2001), "Bearing contact of a helical gear pair with involute teeth pinion and modified circular-arc teeth gear", *Proc. IMechE, Part C: J. Mech. Eng. Sci*., **215**, 1175-1187.

Harris, T. A. (2001), *Rolling Bearing Analysis*, 4th Edition, John Wiley & Sons, Inc., New York, NY, USA.

Hedlund, J. and Lehtovaara, A. (2007), "Modeling of helical gear contact with tooth deflection", *Tribol. Int*., **40**, 613-619.

Hotait, M.A., Talbot, D. and Kahraman, A. (2007), "An investigation of the influence of shaft misalignments on bending stresses of helical gear with lead crown", *Proceedings of the ASME 2007 International Design Engineering Technical Conferences & Computers and Information in Engineering Conference*, Las Vegas, Nevada, USA, September.

Kar, C. and Mohanty, A.R. (2008), "Determination of time-varying contact length, friction force, torque and forces at the bearings in a helical gear system", *J. Sound Vib*., **309**, 307-319.

Kolivand, M. and Kahraman, A. (2011), "A general approach to locate instantaneous contact lines of gears using surface of roll angle", *J. Mech. Des*., **133**, 014503.

Litvin, F.L., Lu, J., Townsend, D.P. and Howkins, M. (1999), "Computerized simulation of meshing of conventional helical involute gears and modification of geometry", *Mech. Mach. Theory*, **34**, 123-147.

Litvin, F.L., Fuentes, A., Gonzalez-Perez, I., Carvenali, L., Kawasaki, K. and Handschuh, R.F. (2003), "Modified involute helical gears: computerized design, simulation of meshing and stress analysis", *Comput. Meth. Appl. M*, **192**, 3619-3655.

Litvin, F.L. and Fuentes, A. (2004), *Gear Geometry and Applied Theory*, 2nd Edition, Cambridge University

Press, Cambridge, England, UK.
Litvin, F.L., Gonzalez-Perez, I., Fuentes, A., Vecchiato, D. and Sep, T.M. (2005), "Generalized concept of meshing and contact of involute crossed helical gears and its application", *Comput. Method Appl. M*, **194**, 3710-3745.
Litvin, F.L., Gonzalez-Perez, I., Fuentes, A., Hayasaka, K. and Yukishima, K. (2005), "Topology of modified surfaces of involute helical gears with line contact developed for improvement of bearing contact, reduction of transmission errors, and stress analysis", *Math. Comput. Model.*, **42**, 1063-1078.
Miyoshi, Y., Tobisawa, K. and Saiki, K. (2007), "Composite analysis method of tooth contact load distribution of helical gear", *Proceedings of the ASME 2007 International Design Engineering Technical Conferences & Computers and Information in Engineering Conference*, Las Vegas, Nevada, USA, September.
Vinayak, H. and Singh, R. (1998), "Multi-body dynamics and modal analysis of compliant gear bodies", *J. Sound Vib*., **210**, 171-214.
Wink, C.H. and Serpa, A.L. (2008), "Performance assessment of solution methods for load distribution problem of gear teeth", *Mech. Mach. Theory*, **43**, 80-94.
Wang, J., Lim, T.C. and Ding, Y. (2012), "Multi-tooth contact behavior of helical gear applying modified meshing equation", *Proc. IMechE, Part C: J. Mech. Eng. Sci*., **227**(1), 146-160.
Wu, S.H. and Tsai, S.J. (2009), "Contact stress analysis of skew conical involute gear drives in approximate line contact", *Mech. Mach. Theory*, **44**, 1658-1676.
Zhang, Y. and Fang, Z. (1999), "Analysis of tooth contact and load distribution of helical gears with crossed axes", *Mech. Mach. Theory*, **34**, 41-57.

CC